Combining DC and AC electric fields with Deterministic Lateral Displacement for Micro- and Nano-particle separation

Victor Calero Martin [a], Pablo Garcia-Sanchez [b], Antonio Ramos [b] and Hywel Morgan [a]*

[a] School of Electronics and Computer Science, University of Southampton, SO17 1BJ, United Kingdom.

[b] Departamento de Electrónica y Electromagnetismo, Facultad de Física, Universidad de Sevilla, 41012, Spain.

* Corresponding author: hm@ecs.soton.ac.uk

Abstract

This paper describes the behaviour of particles in a Deterministic Lateral Displacement (DLD) separation device with DC and AC electric fields applied orthogonal to the fluid flow. As a proof of principle, we demonstrate tunable micro- and nano- particle separation and fractionation depending on both particle size and zeta potential. DLD is a microfluidic technique that performs size-based binary separation of particles in a continuous flow. Here, we explore how the application of both DC and AC electric fields (separate or together) can be used to improve separation in a DLD device. We show that particles significantly smaller than the critical diameter of the device can be efficiently separated by applying orthogonal electric fields. Following the application of a DC voltage, Faradaic processes at the electrodes cause local changes in medium conductivity. This conductivity change creates an electric field gradient across the channel that results in a non-uniform electrophoretic velocity orthogonal to the primary flow direction. This phenomenon causes particles to focus into tight bands as they flow along the channel countering the effect of particle diffusion. It is shown that the final lateral displacement of particles depends on both particle size and zeta potential. Experiments with six different types of negatively charged particles and five different sizes (from 100 nm to 3 µm) and different zeta potential demonstrate how a DC electric field combined with AC electric fields (that causes negative-dielectrophoresis particle deviation) could be used for fractionation of particles on the nano-scale in micro-scale devices.

Introduction

Separation of particles is often a pre-requisite for the analysis of biological samples that are heterogeneous mixtures containing for example cells, vesicles and macromolecules. Microfluidic particle separation has many advantages over standard techniques. Due to the small dimensions of the devices, microfluidic based separation techniques are faster, cheaper and can process much smaller amounts of sample and reagents. They also allow the control of the forces on the particles at the micro-meter scale and can be integrated within Lab-on-a-Chip platforms to deliver complete processing and analysis solutions for diagnostics[1,2].

Deterministic Lateral Displacement (DLD)[3–5] is one of such microfluidic sorting techniques. This method separates particles in the range of micrometres based on size in a continuous flow. DLD devices consist of a microchannel within which there is an array of micro-posts. The rows of the micro-post array are tilted at a small angle (typically <6°) such that particles bigger than a threshold size (termed "critical diameter" or D_c) bump on the posts and deviate while particles smaller than the critical diameter follow the fluid flow, zigzag around the posts, in an overall straight trajectory.

As the particles are dragged by the fluid through the DLD array, they interact with the posts and this interaction determines their paths. The separation mechanism of DLD relies on laminar flow, more specifically in the "separatrix streamlines" as depicted in Figure 1. These streamlines (black line in Figure 1) separate the portion of fluid that passes below, and above a given post (dark post in Figure 1). The separation mechanism occurs when the particles interact with the previous post. When the particles bigger than D_c encounter the previous post, they are pushed and cross the streamline towards the portion of fluid that passes above the post (dark post). In contrast, particles smaller than D_c flow straight following the fluid laminae around the post and remain in the portion of fluid that passes below the post (dark post)[6]. This process is repeated every time the particles interact with a post and the separation is magnified. The big particles flow bumping on the posts and are displaced relative to the small particles that zig-zag around them, resulting in a binary separation. At the end of the device, particles bigger than D_c reach the outlet having been displaced laterally within the device, while smaller particles reach the outlet with no lateral deflection (i.e. they remain in the same streamlines as when they entered the device).

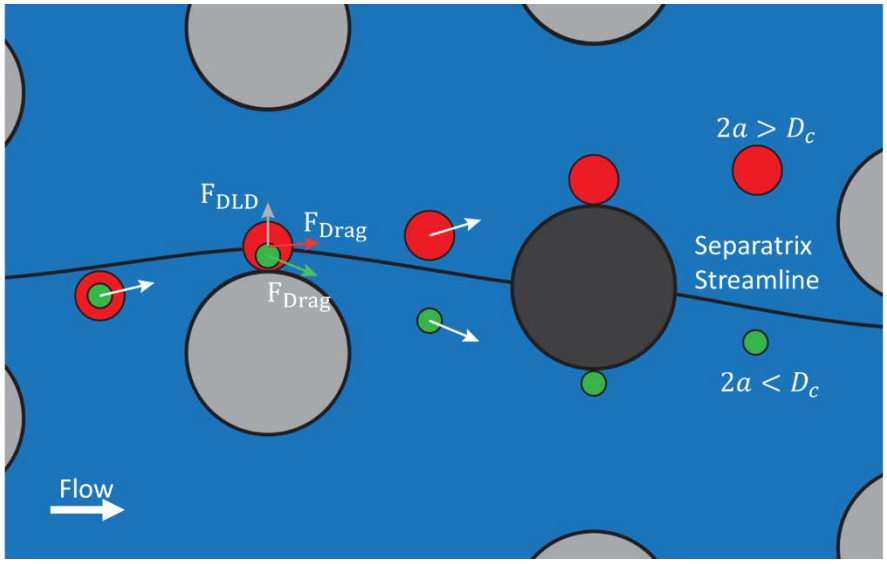

Figure 1. Diagram of the DLD separation mechanism. When the particles encounter a post, they are separated depending on size. Particles bigger than the critical diameter D_c (red) cross the separatrix streamline, passing above the post while particles smaller than the D_c (green) remains within the same fluid lamina, passing above the post. This process is repeated every time the particles interact with a post resulting in a lateral separation between the two types of particles.

The critical diameter (D_c) only depends on the geometry of the micro-post array. Davis derived an empirical formula to estimate D_c for circular posts from the geometry of the array[7]:

$$D_c = 1.4GN^{-0.48} \quad (1)$$

where G is the gap between the posts and N the periodicity of the array, a unit-less parameter that accounts for the number of columns between two columns in the same position.

Since first reported in 2004 by Huang *et al.*[3], the possibilities of DLD have been widely explored[8]. Changes in the geometry of the post array can result in improved separation. Several groups have shown how the use of non-cylindrical posts like triangular[9,10] or I-shaped posts[11,12], improves separation efficiency and enables the separation of non-spherical particles. Different lateral and horizontal gaps between the posts can also lead to enhanced efficiency and throughput over the classic symmetric DLD devices[13].

However, DLD separation has some drawbacks. In principle, it only allows binary size-based separation. Some groups have reported separation based on other properties like cell deformability[14], but the range of applications is still very limited due to the strong dependence on particle size. In addition, the fact that the critical diameter D_c is "hard-wired" by the array geometry means that the value of D_c for any given device cannot be modified. Once fabricated, a device can only be used for a specific set of particle sizes. One way to overcome this restriction was demonstrated by Beech *et al.* who showed how mechanically modifying the dimensions of the DLD array using elastomeric devices fabricated in PDMS can lead to tuneable particle separation[15].

The throughput of DLD devices is low compared to other microfluidic separation techniques like inertial focusing[16] or Pinched Flow Fractionations (PFF)[17] due to the high hydrodynamic resistance that these devices present[18,19]. Nevertheless, this disadvantage is compensated by the high resolution and precision of DLD. A significant challenge is posed by the need to separate sub-micron particles such as extracellular vesicles like exosomes. It has been shown that the device geometry can be scaled down for separation of nanoparticles[20] but the dimensions of the channels become so small that the decrease in the throughput (and high back pressure) makes the device difficult to use. To compensate for this many nanoscale DLD devices can be run in parallel but device fabrication, design and performance remains a challenge[21].

To improve the utility of DLD and increase the range of potential applications, external fields can be imposed on the particles to modify their trajectories as they flow through the array. For example, Devendra *et al.*[22] showed how gravity can be used to tune the separation of particles in the DLD. Beech *et al.*[23] demonstrated that low-frequency AC electric fields applied along the DLD channel in the direction of flow leads to separation of particles smaller than the critical diameter. More recently, the same group reported the use of metal-coated DLD posts to improve this technique[24], reducing the voltage requirements and the minimum particle size that could be separated at the expense of a more expensive and challenging device fabrication. In a recent publication[25], we showed how AC electric fields applied orthogonal to the fluid flow can lead to significant and controlled deviation of particles smaller than the critical diameter through the action of a combination of different electrokinetic forces including Electrophoresis (EP) and

Dielectrophoresis (DEP). Here we present an improvement on this technique, where a combination of orthogonal DC and AC electric fields provides an additional tunable parameter that enables nanoparticle separation and fractionation in a device with micron-sized critical diameter. The DC electric fields cause particles to move by electrophoresis which enables separation based on zeta-potential and significantly reduces the minimum size of particles that can be sorted.

Electrokinetic biased DLD

In previous work[25], we described the effects of applying an AC electric field orthogonal to the fluid flow on particle trajectories through the DLD, and how this can be used to switch the behaviour of particles smaller than the critical diameter from zigzag to bump mode, thus creating a tunable device where separation depends on the applied AC voltage and frequency.

When a high frequency AC electric field is applied to a suspension of particles in an electrolyte, the dominant electrokinetic force is DEP. The presence of the insulating posts in the DLD device distorts the field similar to the well-known insulator-based dielectrophoresis (iDEP)[26], where PDMS posts create regions of high and low electric field gradients between the posts. This gives rise to regions of positive and negative DEP (pDEP and nDEP, respectively) force around the pillars. In the DLD devices used in this work, the AC fields were generated using parallel planar electrodes fabricated along the long edges of the channel as shown in Figure 3. This establishes high electric field gradient regions between posts of the same row. Particles less polarisable than the medium exhibit nDEP and are pushed away from these regions as they flow through the device as explained previously[25]. If the magnitude of the electric field is high enough for the DEP force to overcome the fluid drag force, particles are prevented from passing between the posts in zigzag mode and start bumping onto the posts, deviating at the angle of the posts. This mechanism is described diagrammatically in Figure 2a, where a simulated trajectory for a 1 μm particle experiencing nDEP in a 6.3 μm D_c is shown.

At low frequencies the behaviour is quite different. Here, electrophoresis (EP) dominates and in an AC field, particles oscillate along the electric field lines at the frequency of the field. This oscillation, possibly combined with other phenomena (like electrokinetic wall repulsion[27]) pushes particles smaller than the critical diameter to deviate, even for electric fields significantly lower than needed for nDEP-induced deviation and for particles experiencing positive DEP (pDEP), see Figure 2b. The mechanism behind this low frequency induced deviation is not yet fully understood.

The addition of a DC component to the AC field can be used to further tune particle separation in the DLD system. A DC electric field exerts a constant EP force on particles, which affects their trajectories. The relationship between the magnitude of the electric field ($\boldsymbol{E}$) and the particle electrophoretic velocity ($\boldsymbol{v}_{EP}$) is given (for thin double layer) by:

$$\boldsymbol{v}_{EP} = \mu_{EP}\boldsymbol{E} \quad (2)$$

where μ_{EP} is the electrophoretic mobility, which in general is:

$$\mu_{EP} = \frac{\varepsilon\zeta}{\eta} \quad (3)$$

ε is the dielectric constant of the suspending medium, η the dynamic viscosity, and ζ the zeta potential of the particle, which is related to the particle fixed charge.

Equation 2 predicts a linear relationship between the electric field magnitude and $\boldsymbol{v}_{EP}$. Although the electric field is distorted by the posts in the DLD, the particle velocity is expected to be uniform overall across the channel section. However, as shown below (results section), we observed that the particle velocity $\boldsymbol{v}_{EP}$ changes with lateral position, depending on proximity to the two Pt electrodes (see Figure 3). We postulate that this effect is due to local changes in electrolyte conductivity near the electrodes caused by the creation of ionic species (Faradaic reactions) when a DC voltage is applied. This effect leads to a region of reduced electric field magnitude near the electrodes which, similar to other observations on electric field gradient focusing[28], causes narrowing of the particle stream and the formation of well-defined bands whose distance from the electrode depends on the electrophoretic mobility (μ_{EP}) of the particles.

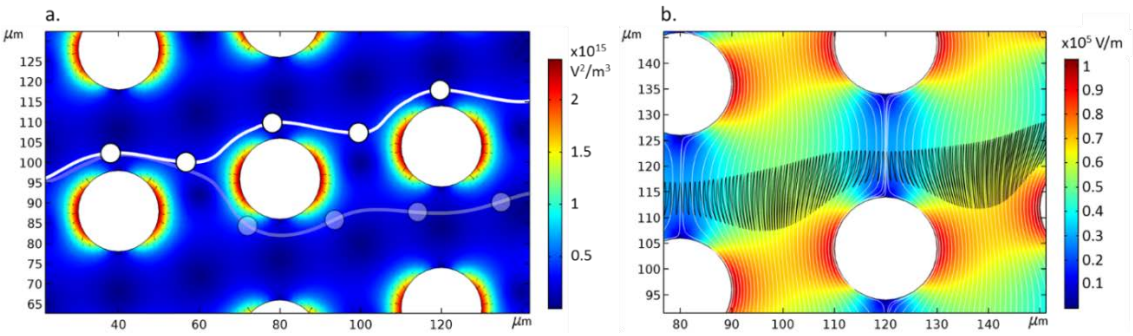

Figure 2. Numerically determined trajectories of particles moving inside a DLD device with an AC electric field applied orthogonal to the direction of fluid flow. Simulation calculate, using the commercial finite element software COMSOL Multiphysics v5.3. (a) nDEP induced deviation of a 1 μm particle in a 6.3 μm D_c DLD. Colours represent the electric field gradient squared and the black arrows the direction of the nDEP force. The white line represents particle trajectories due to nDEP, while the transparent line shows trajectories in the absence of any DEP. (b). Low frequency particle oscillation driven by EP, showing movement along the electric field lines (black lines). Colours represent the magnitude of the electric field, and the white lines the electric field lines.

Materials and methods

DLD devices and experimental setup

A diagram of the DLD devices used for the experiments is shown in Figure 3. The device consisted of a microchannel with a simple DLD array of offset micro-posts with two outlets, one for the deflected particles that bump on the posts and the other for the non-deflected particles that flow straight. Note that in order to achieve a practical particle fractionation it would be necessary to fabricate devices with several outlet channels instead of only two. For ease of use, this device has only two outlets. It has three inlets; the central inlet was used to introduce the sample and the other two are for sheath flow to focus the particles in a stream of roughly the same width as the sample inlet channel. The channel inlet is not positioned in the mid-point of the channel so that the lateral positions of the particles at the inlet and the outlet is maximised and to allow the lateral displacement at the outlet to be measured.

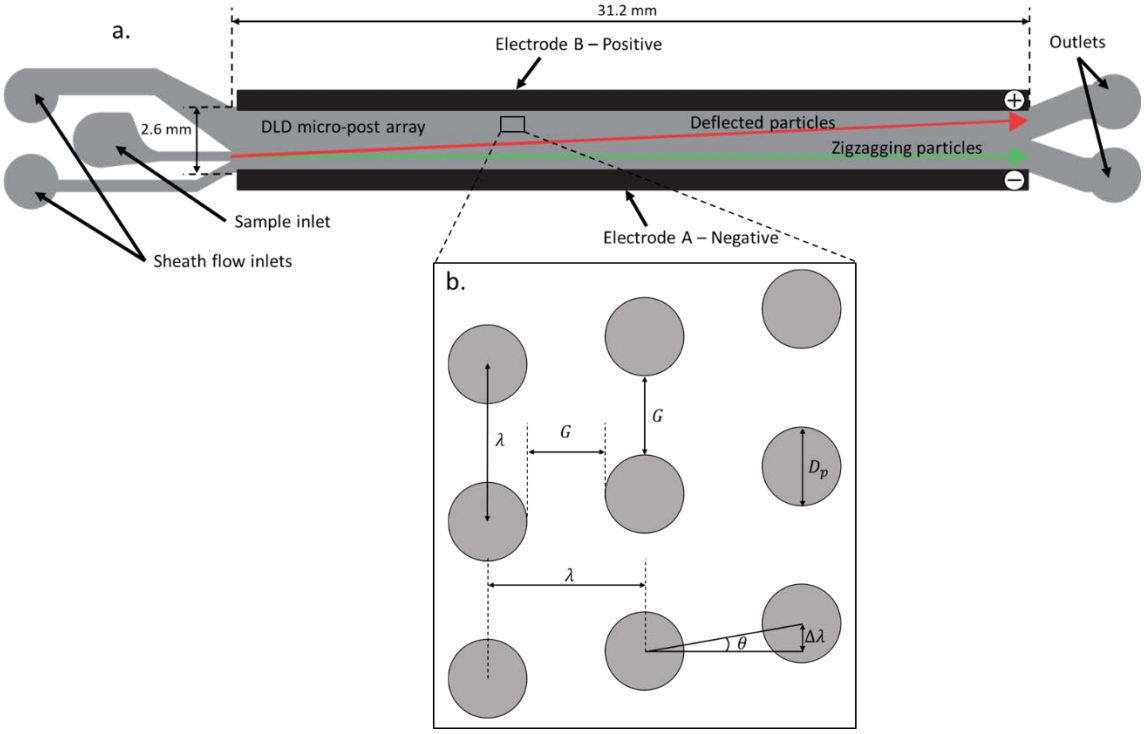

Figure 3. (a) Diagram of a DLD device with integrated Pt electrodes. In the absence of deviation, particles flow straight from inlet to outlet following the green path. However, if the particles are deflected by the posts, they reach the outlet with a certain lateral displacement compared to the starting position (red path). (b) Parameters that define the DLD array geometry.

The DLD device consisted of a symmetric array of offset circular posts with gaps between the posts equal to the post diameter ($D_p = G$, see Figure 3b). With reference to the parameters defined in Figure 3b, two different DLD arrays were used, one with D_p =18 μm, λ=36 μm, θ=3.18º and D_c = 6.3 μm (as given by Equation 1), and another with D_p =15 μm, λ=30 μm, θ=2.86º and D_c =5.0 μm. The height of the channels was approximately 8 μm.

The devices were made from PDMS (polydimethylsiloxane) using a master fabricated by standard photolithography. The PDMS was bonded to a glass slide with patterned platinum electrodes using plasma-activated bonding. The channel was aligned to the two planar parallel electrodes so that the electric field was perpendicular to the fluid flow. The planar electrodes were separated by a gap of 2.2 mm and were 31.3 mm long, so that they covered the entire length of the DLD array. The labelling of the electrodes is shown in Figure 3; Electrode A is the electrode closest to the inlet and electrode B is the electrode to which the particles move when they are deflected (particles are all negatively charged). This convention will be used throughout the paper. The electrodes were connected to a signal generator (TTi, Inc® TGA12104) that applied DC voltages up to ±20 V. For the experiments with AC electric fields, the signal generator was connected to a x50 amplifier (Falco Systems® High Voltage Amplifier WMA-300) to deliver up to 320 Vpp AC. The fluid flow was driven using a pressure controller (Elveflow® OB1 MK3) with three channels to allow an independent and precise flow rate control at each inlet.

Samples

The particles used for the experiments were 100 nm, 200 nm, 500 nm, 1 μm and 3 μm diameter fluorescent carboxylate microspheres (Fluoresbrite® YG Carboxylate Microspheres) and 3 μm diameter plain polystyrene microspheres (Sigma Aldrich). The suspending medium for the particles was KCl diluted in DI water in two different concentrations, with conductivities of 6.6 mS/m and 12.5 mS/m. The PDMS devices were pre-treated with Pluronics F-127 for at least one hour before the experiments to avoid particle adhesion to the channel walls. The zeta potential (ζ) of the particles used for the experiments were measured using a Zetasizer (Malvern Panalytical® Zetasizer Nano ZS) and the results are summarised in table 1.

Particle	3 μm plain	3 μm carboxylate	1 μm carboxylate	500 nm carboxylate	200 nm carboxylate	100 nm carboxylate
ζ (mV)	-15 ± 3	-78 ± 6	-71 ± 4	-63 ± 6	-52 ± 7	-49 ± 7

Table 1. Measured zeta potential (ζ) of the particles used in this wok. They were suspended in diluted KCl with 6.6 mS/m conductivity, the same suspending medium used for the experiments.

Results and discussion

Size-based tunable separation

As described previously, AC electric fields (without any DC) can be used to tune binary separation in DLD devices. Figure 4 shows how the application of a small DC voltage together with an AC signal leads to fractionation of a mixture of different particles. The figure shows a mixture of 1 μm, 500 nm and 100 nm diameter carboxylate spheres separating within a DLD with 6.3 μm D_c, and a 500 Hz (320 Vpp) AC signal combined with a -0.25 V DC applied to the electrodes. The imposed pressure driven fluid flow leads to an average particle velocity of around 50μm/s. In all experiments, the applied DC voltage was always negative with respect to electrode A (bottom electrode in Figure 3) whilst electrode B (top electrode in Figure 3) was grounded.

Figure 4a shows how a mixture of three different particle sizes divides into streams at a mid-point in the channel. Particles continue to separate as they flow along the channel until they reach a maximum lateral deviation and then keep flowing straight towards the outlet. The difference in the lateral displacement translates into a maximum deviation at the outlet resulting in efficient particle fractionation. Figure 4b shows an image of the streams at the outlet of the device

demonstrating fractionation of 1 μm, 500 nm and 100 nm particles. Note that the curved particle streams shown in Figure 4b is an artefact and occurs due to the relative position of the two outlet channels (see Figure 3a).

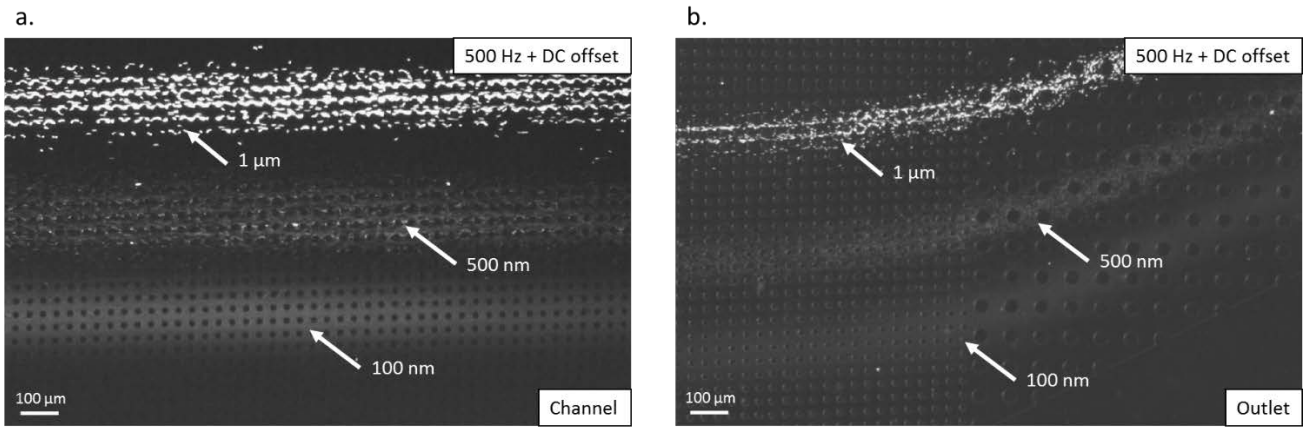

Figure 4. Fluorescent image showing fractionation of a mixture of 1 μm, 500 nm and 100 nm particles suspended in 12.8 mS/m KCl with a 6.3 μm D_c DLD. The applied field was 500 Hz 320 Vpp AC with a superimposed DC offset of -0.25 V (applied to electrode A). (a). Particles move to form bands in the channel. (b). The bands remain with a constant lateral separation until they reach the outlet.

Experiments show that the addition of a DC component provides several advantages over an AC electric field. Classical DLD, or DLD in combination with AC fields only leads to binary separation. One particle type bump on the posts while the other type zigzags around in a straight line leading to separation into two populations. However, by combining a DC electric field with the AC field, more than two different types of particles can be fractionated at the same time, as shown in Figure 4.

Another advantage is that the DC component enables separation of particles much smaller than the critical diameter, i.e. nanoparticles, because the electrophoretic force does not scale with particle size. In our devices, it was not possible to induce any deviation of particles below 500 nm with only an AC signal. Furthermore, as particles separate, it was observed that the DC electric field focuses each type of particle into a narrow stream, minimising the influence of diffusion, which is a significant obstacle to the separation of nanoparticles in microfluidic systems. The mechanism responsible for this is not fully understood yet but to explore this phenomenon further, a mixture of 500 nm, 1 μm and 3 μm carboxylate (negative surface charge) particles were separated in a device with a smaller critical diameter (D_c = 5.0 μm) at different DC voltages. The data is summarised in Figure 5 and shows the larger diameter particles experienced significant electrically induced deflection with increasing flow rates. Note that the data points represent the mean lateral displacement of the stream at the outlet, and the vertical bars on each data point correspond to the stream width. The displacement data were measured far enough from the outlet to ensure the distorted fluid flow observed in Figure 4b did not influence the data.

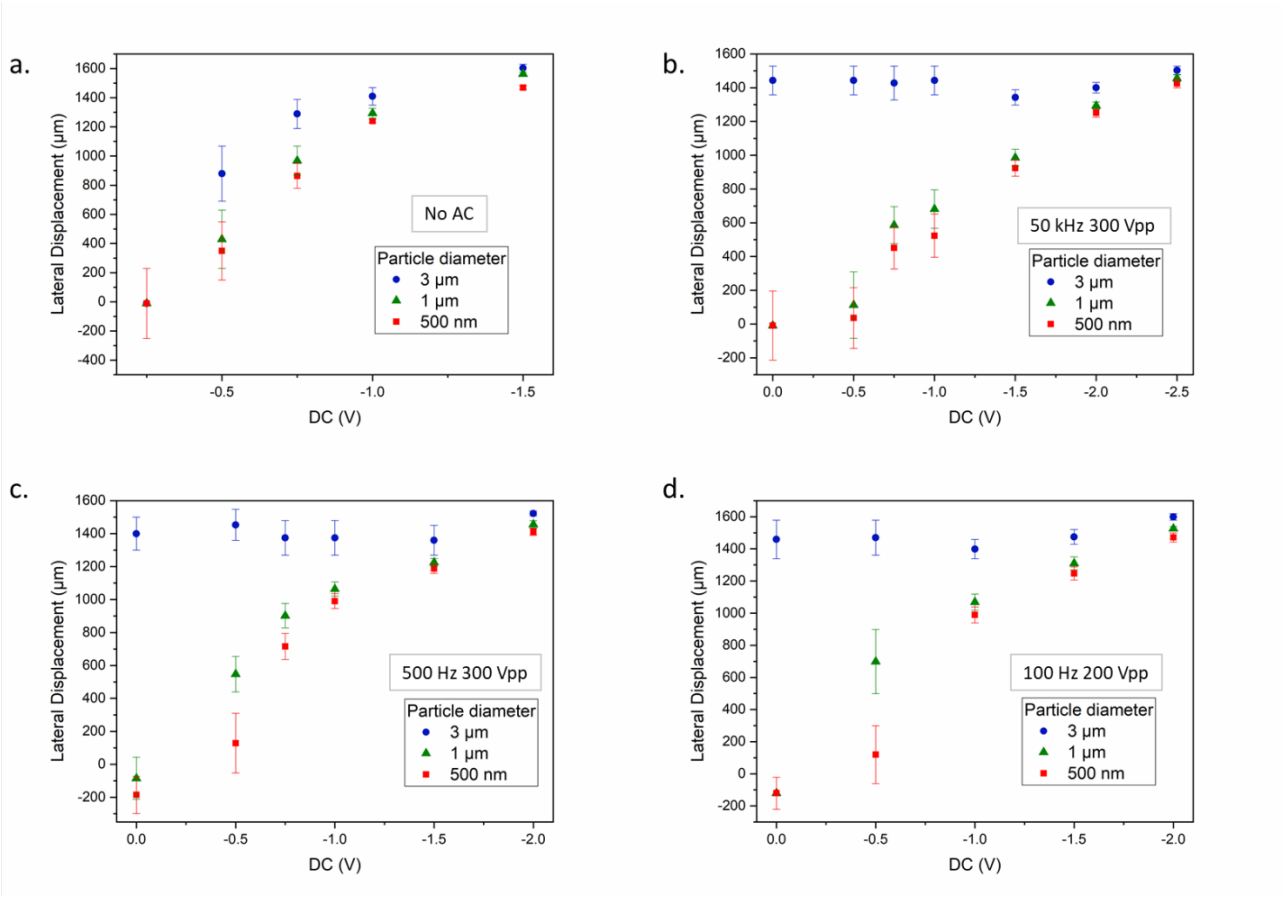

Figure 5. Lateral displacement of a mixture of 500 nm, 1 µm and 3 µm diameter carboxylate spheres in a 5.0 µm D_c DLD using a combination of DC and AC electric fields as a function of the DC voltage applied to electrode A. The vertical bars on the datapoints indicate the width of the particle stream. Flow velocity was approximately 120 µm/s. Particles were suspended in an electrolyte with a conductivity of 6.6 mS/m (a). DC only, no AC. (b). AC: 50 kHz 300 Vpp. (c). AC: 500 Hz 300 Vpp. (d). AC: 100 Hz 320 Vpp.

Figure 5a shows lateral displacement of particles with only a DC voltage and no AC voltage is applied. In this case, the 3 µm particles are separated from the 1 µm and 500 nm particles at voltages between -0.5 V and -1 V. Since all three types of particles are made of the same material and suspended in the same electrolyte, their zeta potentials are very similar (see Table 1). The difference in the zeta potential between the 3 µm and 1 µm particles is approximately the same as the difference between the 1 µm and 500 nm particles. If the separation were only zeta potential dependent, the separation between the 3 µm and 1 µm particles should be the same for the 1 µm and 500 nm particles. However, the data shows size-based separation of 3 µm particles from the smaller particles due to the DC electric field but not significant separation of the 1 µm from the 500 nm particles. This fact might indicate that the DLD posts play an important role in the separation mechanism since it is easier for the DC to induce deviation of the 3 µm particles that are closer to the D_c (5.0 µm). Below -1 V, (i.e. for more negative voltages) separation of the particle streams is marginal and the 3 µm particles can no longer be distinguished from the other sizes. For these higher DC voltages, the lateral positions are almost independent of particle size, in agreement with equation 2. For higher DC voltages, the electrophoretic velocity of all the particles is high and they reach the outlet with the same lateral displacement. There is also a significant overlap between the 1 µm and 500 nm particles for all applied voltages, implying that the array has a similar effect on both these particle sizes, even though the difference in the zeta potential is similar to the difference in the zeta potential between the 3 µm and 1 µm particles

The data also shows that the effect does not scale linearly with DC voltage, counter to that predicted by equation (2). For a constant flow rate and an orthogonal and uniform field and therefore $\boldsymbol{v}_{EP}$, the relationship between the (measured) lateral displacement and the applied DC voltage should be linear. In contrast, Figure 5a shows a sub-linear increase in the lateral displacement when the particles are close to electrode B. This dependence on the proximity to the electrode suggests a non-uniform (DC) $\boldsymbol{v}_{EP}$ across the channel section. A lower $\boldsymbol{v}_{EP}$ is observed near the electrodes compared with the middle of the channel, which translates into a decay in the lateral displacement with applied DC when the particles are close to electrode B. Figure 5a shows that this linearity is lost for lateral displacements beyond 1000 µm.

Figures 5b, 5c and 5d show lateral displacement of particles when both a DC and AC electric field is applied, as a function of the DC voltage. Figure 5b shows that a high frequency (50 kHz) electric field leads to full deflection of the 3 μm particles even in the absence of DC due to the action of a nDEP force, as described in our previous publication[25]. However, the DEP force produced by the same AC field was unable to deviate the smaller 1μm and 500 nm particles. At the flow rate used in this experiment, the DEP force acting on these particles was too small (DEP velocity scales with square of radius) to induce any significant deflection and push particles across the separatrix streamline. These particles only deflected when a DC component was applied. However, similar to the case with no AC voltage (Figure 5(a)), particles were not separated and the overlap between the two populations was large for all DC voltages.

Figure 5c and 5d show how a low frequency (<1 kHz) AC electric field, combined with a small DC voltage leads to separation of not only the 3 μm particles from the smaller populations, but also separation of the 1 μm and 500 nm particles, i.e. the mixture was fractionated. This contrasts to Figure 5a where only a DC voltage was applied. The presence of the DC voltage leads to the superposition of a constant electrophoretic force on top of the low-frequency oscillating AC electrophoretic force. As shown in the figures, the optimal DC fractionation voltage is -0.5 V since at this point the 1 μm diameter particles are deflected, but the voltage is not high enough to induce deviation of the 500 nm particles. The low frequency driven deviation strongly depends on size but is too weak for the 500 nm particles so that the DC voltage is not high enough to induce deflection and the particles do not deviate significantly. For higher voltages the force is always high enough for both types of particles to achieve a significant and very similar lateral displacement, thus separation is no longer observed. As shown in Figure 4, application of a DC voltage focuses the particles into a tight stream, effectively damping diffusion. This can be seen in the vertical bars in Figure 5. This effect becomes more prominent as the DC voltage and lateral displacement increase, possibly due to electrophoretic velocity that depends on the lateral position.

DC induced deviation and focusing of 200 nm spheres

To further investigate the effects of the DC voltage on particle trajectories, experiments were performed with 200 nm diameter fluorescent carboxylate nanospheres that are almost unaffected by the presence of the tilted array of posts. For consistency the pressures were kept the same, delivering the same fluid flow speed in the channel. Images of particle behaviour and a summary of the results are shown in Figure 6. In the experiments, the sheath flow and inlet pressures were adjusted to achieve a stream width similar to the width of the inlet channel (300 μm). Figure 6a) shows the width of a 200 nm particle stream immediately after entering the DLD channel. The inlet is close to the lower part of the channel, near electrode A (see Figure 3) so that the net lateral displacement of the particle stream can be quantified by comparing the position of the stream at the outlet with the position at the inlet.

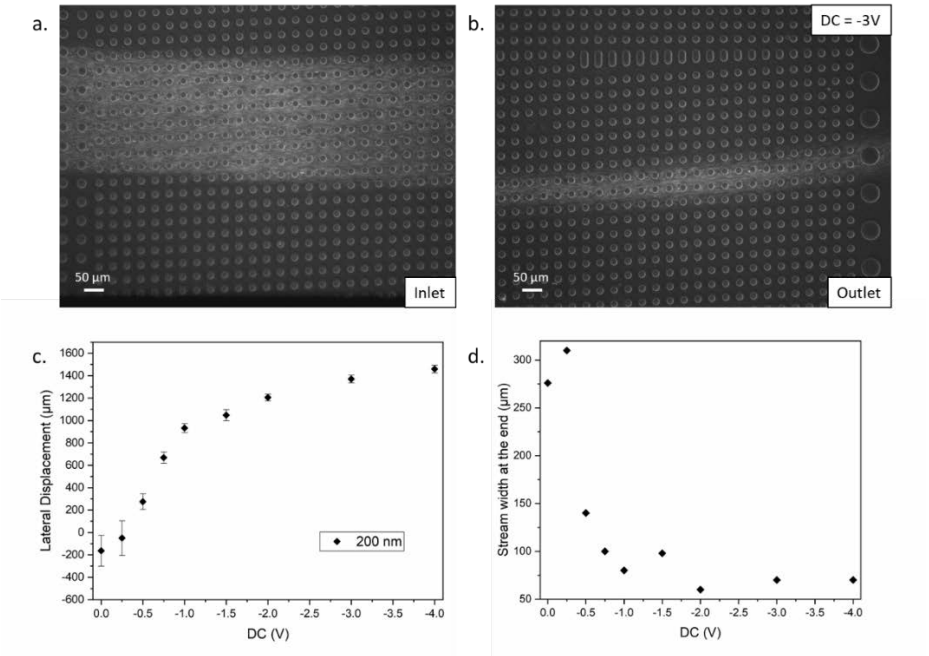

Figure 6. (a). Fluorescent image of a stream of 200 nm diameter particles moving through the DLD device under a pressure driven flow. Particles were suspended in a 1.4 mS/m KCl solution. The particles enter the device with a uniform fluorescence intensity across the stream corresponding to a width of 300 μm. (b). Image showing the same 200 nm diameter particle stream focused into a much narrower band after being displaced closer to electrode B at the outlet of

the channel. Applied DC voltage of -3 V DC to electrode A. (c). Particle stream deviation measured near the channel outlet plotted as a function of the applied DC voltage (reference to electrode A. The vertical bars indicate the width of the particle stream. (d). Particle stream width as a function of the applied DC voltage showing the significant focusing effect of the applied potential.

Figure 6b shows the effect of applying a -3 V DC voltage to electrode A and the resulting change in width of the particle stream at the outlet of the device close to electrode B. The DC voltage has two main effects on the trajectories of the 200 nm diameter particles (compare Figures 6a and 6b). First, electrophoresis pushes the negatively charged nanoparticles away from electrode A towards electrode B as they flow towards the outlet, resulting in a significant lateral displacement. The final lateral position of the particle stream depends on the applied DC voltage. Secondly, the width of the particle stream is significantly reduced at the outlet compared with the width at the inlet. For the 200 nm particles, the stream is expected to widen as the particles flow through the device due to diffusion. The mean displacement of a solid particle due to diffusion in an aqueous suspension (in one dimension) is given by:

$$\bar{x} = \sqrt{2Dt} \quad (4)$$

where D is the diffusion constant and t the time. From this equation, it is possible to estimate that the 200 nm particle stream should diffuse by approximately 80 μm at the flow velocity stated above. However, as shown in Figure 6b the applied voltage leads to focusing of the particle stream, counteracting the effect of diffusion.

Figure 6c and 6d provide detailed experimental measurements of these effects. Figure 6c shows a non-linear dependence of displacement with electric field, counter to the simple model that implies a uniform $\boldsymbol{v}_{EP}$ across the channel section, as observed for bigger particles. As the applied DC voltage increases, the degree of lateral displacement decreases as shown in Figure 6c. The bars in Figure 6c and Figure 6d show how the width of the particle stream is significantly reduced when the applied DC voltage at electrode A is above -0.25 V.

Both results suggest that there is a decrease in the electric field magnitude in the regions near the electrode. Observation of the particles as they travel along the DLD channel shows that $\boldsymbol{v}_{EP}$ changes as the particles approach the electrodes. Particles in the centre of the channel have a significantly higher $\boldsymbol{v}_{EP}$ than particles near the electrodes, consistent with a gradient in the electric field across the channel width as discussed previously. When particles are subjected to a low frequency AC in combination with the DC, it was also observed that the oscillation amplitude reduces near the electrodes.

Zeta-potential based separation

Separation of particles based on zeta potential was demonstrated with a mixture of two different types of particles with the same size but different zeta potentials. 3 μm diameter carboxylate (fluorescent) microspheres with ζ=-78 ± 6 mV and 3μm plain polystyrene microspheres with ζ=-15 ± 3 mV were separated using a 5.0 μm D_c DLD. Carboxylate particles have a high negative surface charge whereas the plain polystyrene microspheres are only slightly negatively charged, resulting in different zeta potentials.

Figure 7a shows images of the evolution of the particle streams as particles flow through the DLD device in the presence of a low frequency AC electric field together with a negative DC voltage. When particles first enter the channel, they flow together in a single stream with width equal to the inlet channel (Figure 7a). As they continue along the channel, they are deflected towards the upper electrode (B) but are separated by the electric field into two different streams that continue to flow in parallel with almost zero deviation (Figure 7b). At the outlet, both particle populations have different lateral displacement but also a significant reduction in the width of the sample stream is observed. The electric field both reduces diffusion and drives separation (Figure 7c). The effects of the deviation of the streams at the outlet channels can be seen.

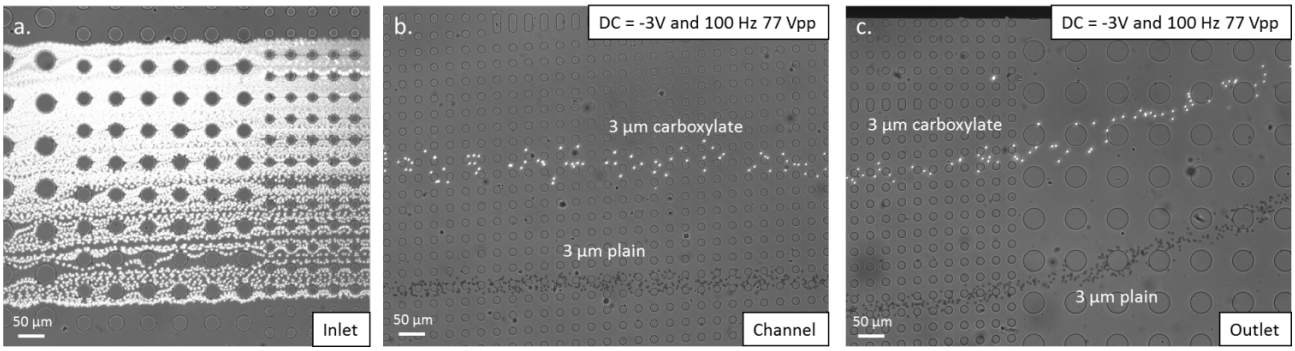

Figure 7. Fluorescent images showing separation of a mixture of 3 μm fluorescent carboxylate and 3 μm plain microspheres in a 6.3 μm D_c DLD with a 6.6 mS/m KCl suspending medium. The applied peak-to-peak voltage was

77 Vpp AC at 100 Hz, combined with -3 V DC applied to electrode A. (a). The 3 μm carboxylate and 3 μm plain particles enter the channel together in a stream with a width similar to the dimensions of the inlet. (b). As the particles flow through the channel, both populations are deflected, separated and focused into tight streams that flow almost straight and close to electrode B. The bright dots correspond to the carboxylate spheres (fluorescent) and the dark dots to the plain spheres. The picture was taken at a mid-point in the channel. (c). This behaviour results in separation that is a function of particle zeta potential. Particles with a more negative zeta potential reach the outlet having experienced a larger lateral displacement. Note that the three images were all taken with the same magnification.

Figure 8(a) shows how the zeta potential based separation varies as a function of the negative DC applied to electrode A in the absence of any applied AC. Although the carboxylate particles undergo a larger displacement compared to the plain spheres at any applied voltage, the overlap between the two populations is still significant at low voltages. A clear separation only occurs for voltages above -2V. This plot also shows that the displacement becomes non-linear with DC voltage when the particles are close enough to the electrode, due to the non-uniformity of the $\boldsymbol{v}_{EP}$.

When a combination of DC plus AC voltage is used, separation between the two populations is much clearer even at lower DC voltages. Figures 8b and 8c show the effect of combining the DC with either a 50 kHz or 100 Hz AC voltage respectively. In both cases, the AC voltage was kept low in order to minimise deviation due to either nDEP or low-frequency EP, but high enough to lead to a measurable effect when combined with a DC. At high frequencies, the same DEP strength is expected for both types of particles, but the DC voltage acts together with the AC to deflect and separate the particles; the separation is distinct due to the field-induced focusing of the particle streams. This is illustrated by the bars of Figure 8b where there is no overlap between the two populations of particles for voltages above -1 V. The effect of the AC is more evident at low frequencies (Figure 8c) since the electrophoretic mobility is more important for a low frequency AC induced separation. The combination of a -0.5 V DC with 100 Hz 77 Vpp AC leads to significant deviation of the carboxylate particles while there is almost no deviation of the plain polystyrene microspheres.

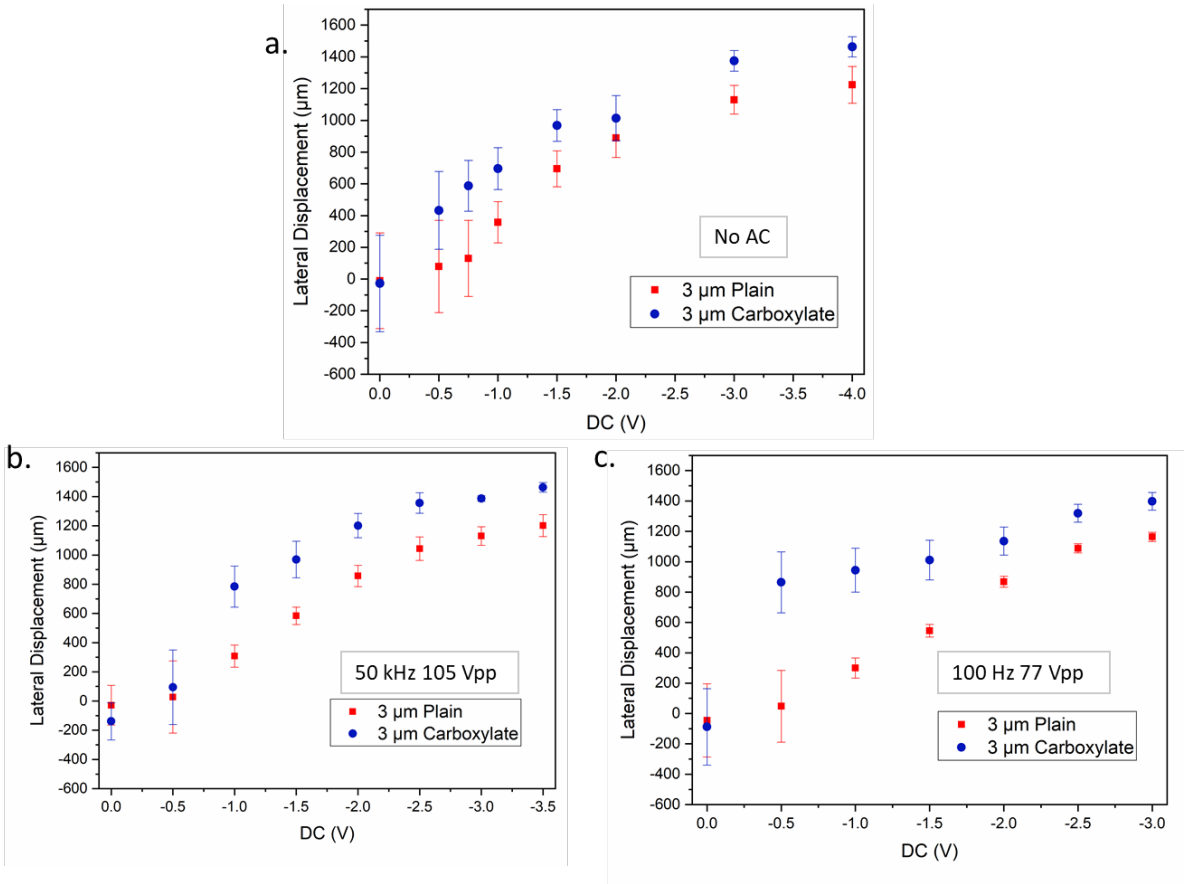

Figure 8. Zeta potential based separation of 3 μm fluorescent carboxylate and 3μm plain microspheres in a 6.3 μm D_c DLD using a combination of DC and AC electric fields, as a function of the applied DC voltage to electrode A. The bars represent the measured width of the particle stream. Electrolyte (KCl) conductivity = 6.6 mS/m (a). Negative DC voltage only. (b) DC combined with a 50 kHz 105 Vpp AC electric field. (c) DC combined with a 100 Hz 77 Vpp AC electric field.

Electric field gradients and particle bands

Experiments were undertaken in the absence of any pressure driven fluid flow in order to understand the effects of the DC field on particle behaviour. Equation (2) shows that for a uniform electric field, any particle with a given zeta potential is expected to move with a constant electrophoretic velocity. Nevertheless, as previously discussed, a DC field applied orthogonal to the main flow leads to a particle electrophoretic velocity that depends on position relative to the electrodes.

All the particles are negatively charged so that when a negative DC voltage is applied to electrode A, they should all move away from this electrode and migrate towards electrode B at a uniform speed. Experimentally a lateral velocity gradient is established such that particles closest to the electrodes travel slower than particles in the centre of the channel. As a result, particles have a lower residence time in the centre. Due to the relative difference in velocities, the particles concentrate in narrow bands close to electrode B. At the same time, they continue to move slowly towards the electrode it down the much lower field gradient. Figure 9a shows banding of 500 nm, 200 nm and 100 nm diameter particles with -1 V DC applied to electrode A. Particles that were initially uniformly distributed over the width of the channel form well defined bands parallel to the electrodes when the voltage is applied. All the particles that were closer to electrode A move into the band, but the particles initially located near electrode B remain outside the band. This is due to the absence of any driving force to move the particles away from electrode B.

Figure 9b shows the band pattern which emerges when 1 µm and 500 nm particles are initially located close to electrode A. In this arrangement, with -2 V DC applied to electrode A, the final bands are closer to electrode B than the initial position of any of the particles. This enables all the particles to migrate in this direction as seen in Figure 9b, resulting in the formation of distinct bands of each particle size. These particle size-dependent bands exist due to the faster movement of larger particles towards electrode B. This may arise from small differences in electrophoretic mobility and/or the interaction of the particles with the posts as they cross the channel. Due to the well-defined starting position of the particles, the bands are distinct from one another and do not merge into a single stream as seen in Figure 9a.

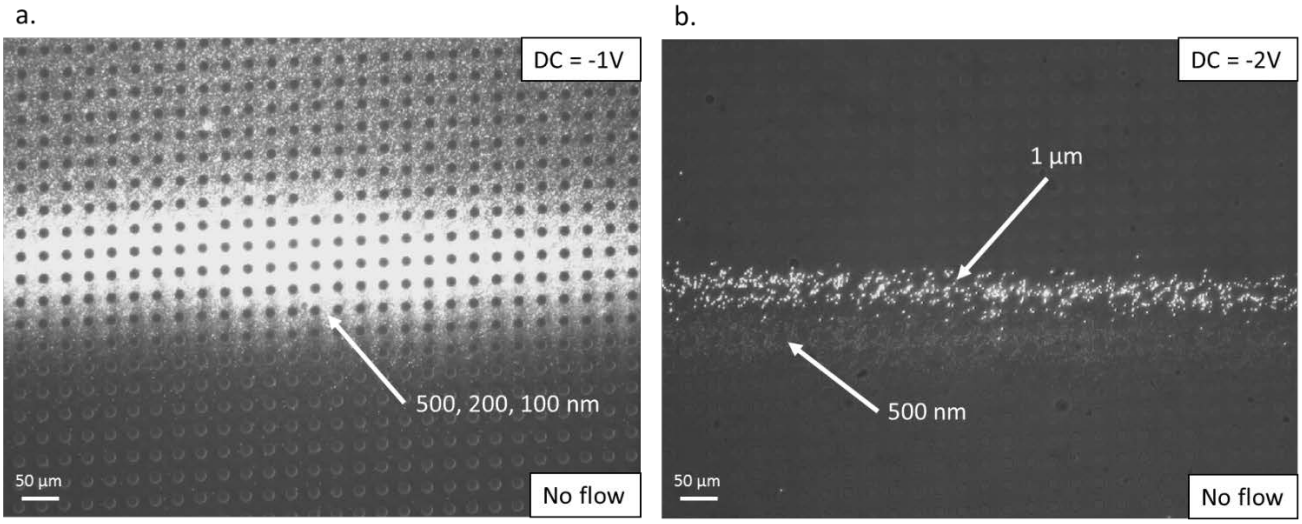

Figure 9. Formation of particle bands. (a). One stream of 500 nm, 200 nm and 100 nm particles initially spread all over the channel section when -1V DC is applied to electrode A. Above the band (near electrode B), the particles do not move due to the low electric field magnitude. Below the band, particle depletion is observed. (b). Two bands of 1 µm and 500 nm particles formed when -2 V DC was applied to electrode A. The particles were initially close to the bottom electrode (A) but then concentrated into bands positioned at different lateral positions, possibly due to small differences in the electrophoretic mobility.

These effects can be attributed to local changes in the medium conductivity caused by the applied DC voltage. This effect is similar to the mechanism underlying isotachophoresis which is used for separation and concentration of analytes[29,30]. As described in an earlier publication describing fluid flow in microchannels driven by a combination of DC and AC voltages[31], when a voltage is applied to an electrode, electrochemical reactions occur at the electrode surface to maintain an electric current. These electrochemical reactions release ions into the solution that modify the local conductivity in the regions near the electrodes leading to changes in the electrokinetic behaviour. A region of enhanced conductivity means a reduced resistivity and thus a reduced voltage drop. This results in a decrease in the electric field magnitude near the electrodes, reducing the electrophoretic force and thus the particle velocity.

When a negative DC voltage is applied to electrode A, any particles close to the inlet and near this electrode have a large $\boldsymbol{v}_{EP}$ and are pushed away before any Faradaic reaction products at the electrode changes the local conductivity. At

electrode B, a combination of diffusion of the electrochemically produced ions into the bulk solution and the electrophoretic mobility of the particles determine the position of the band. The quicker the particles move the farther they can travel until they reach the diffusing ions and the region of minimum electric field.

In the presence of an imposed fluid flow, a higher electric field in the centre of the channel compared to near the electrodes translates into a fast lateral $\boldsymbol{v}_{EP}$ when particles enter the channel. Particles move quickly across the device and rapidly reach a region of low electric field where they concentrate in a tight band and then continue flowing almost in parallel to the electrode due to the very low lateral $\boldsymbol{v}_{EP}$, until they exit the device. The fact that the particles displace slowly until the end of the device means that this band remains focused, overcoming diffusion. Any particle that diffuses towards electrode B reaches a region where $\boldsymbol{v}_{EP}$ is low, while the rest of particles in the stream have a higher $\boldsymbol{v}_{EP}$. The main stream of particles quickly reaches the position of this particle and continues flowing. Any particle that diffuses towards the middle of the channel is pushed back into the main stream by the higher $\boldsymbol{v}_{EP}$ in this region. A similar focusing mechanism using a single spatially varying electric field is described in reference [32].

Conclusions and outlook

In this paper we presented a new DLD configuration that combines orthogonal AC and DC electric fields to increase the tunability and separation of particles much smaller than the critical diameter. Our previous work[25] showed how separation could be enhanced using AC electric fields. Here we demonstrate the effect of adding a DC component and demonstrate that an electrophoretic force orthogonal to the main flow confers several advantages over classical DLD or AC tuned DLD separation, leading to new ways of controlling particle separation including based on particle zeta potential.

The addition of a DC component confers additional functionality by converting a binary separation system into a particle fractionation device. It also enables separation of much smaller particles using comparably large pillar diameters. Experimental data of lateral displacement demonstrates not only that 3 µm spheres can be separated from smaller particles using a pure DC electric field, but also that a mixture of 3 µm, 1 µm and 500 nm spheres can be successfully fractionated in a 5.0 µm D_c DLD. We also show how a DC field can be used to significantly reduce the minimum size of particles that can be deflected due to the independence of EP with particle size. This was demonstrated by the deflection of 200 nm particles and the separation 100 nm from 500 nm and 1 µm particles using a DC field. This behaviour does not occur using a pure AC electric field due to the strong dependence of the DEP force on particle size. Furthermore, the force is independent of particle shape, making this technique applicable to a much wider range of particle types. Application of a DC electric field not only expands the range of possibilities of size-based separation but also enables separation based on particle zeta potential, as shown using 3 µm carboxylate charged and 3 µm plain polystyrene microspheres. In principle this could be extended to the fractionation of nanometre particles of different functionality.

The separation mechanism is significantly affected by the production of ionic species at the electrodes, caused by Faradaic reactions due to the applied DC voltage. This locally increases the conductivity near the electrodes, and these conductivity gradients translate into gradients in electric field magnitude. These gradients in electric field are orthogonal to the fluid flow and lead to tight focusing of particles, overcoming diffusion and enhancing the purity and resolution of the separation. This makes the technique ideally suited to nanoparticle separation but with the advantage of large pillar sizes which are easy to manufacture, with high flow rates/throughput and low back pressure. Particle fractionation is attributed to the electric field gradients that occur near the electrodes. In the present experimental design, these conductivity changes occur in an uncontrolled environment so that the electrochemical reactions, the amount and rate of released ions and their effect in the conductivity are hard to characterise. New designs would provide better control of these parameters.

The experimental data shows improved separation when a DC voltage is combined with an AC electric field. However, a full understanding of the mechanisms underlying these observations will be the subject of future work. Both theoretical and numerical analysis should provide new insights into the underlying mechanisms leading to the design of improved particle separation and fractionation technologies.

Conflict of interest

The authors declare no conflict of interest.

Acknowledgments

P.G.S. and A.R. acknowledge financial support from Spanish Government Ministry MICINN under Contract No. PGC2018-099217-B-I00.

References

1 A. A. S. Bhagat, H. Bow, H. W. Hou, S. J. Tan, J. Han and C. T. Lim, *Med. Biol. Eng. Comput.*, 2010, **48**, 999–1014.

2 D. R. Gossett, W. M. Weaver, A. J. MacH, S. C. Hur, H. T. K. Tse, W. Lee, H. Amini and D. Di Carlo, *Anal. Bioanal. Chem.*, 2010, **397**, 3249–3267.

3 L. R. Huang, E. C. Cox, R. H. Austin and J. C. Sturm, *Science (80-.).*, 2004, **304**, 987–990.

4 D. W. Inglis, J. A. Davis, R. H. Austin and J. C. Sturm, *Lab Chip*, 2006, **6**, 655–658.

5 D. W. Inglis, *Appl. Phys. Lett.*, 2009, **94**, 013510.

6 S. Kim, B. H. Wunsch, H. Hu, J. T. Smith, R. H. Austin and G. Stolovitzky, *Proc. Natl. Acad. Sci.*, 2017, **114**, E5034–E5041.

7 J. A. Davis, Princeton University, 2008.

8 J. McGrath, M. Jimenez and H. Bridle, *Lab Chip*, 2014, **14**, 4139–4158.

9 K. Loutherback, K. S. Chou, J. Newman, J. Puchalla, R. H. Austin and J. C. Sturm, *Microfluid. Nanofluidics*, 2010, **9**, 1143–1149.

10 Z. Liu, F. Huang, J. Du, W. Shu, H. Feng, X. Xu and Y. Chen, *Biomicrofluidics*, 2013, **7**, 11801.

11 K. K. Zeming, S. Ranjan and Y. Zhang, *Nat. Commun.*, 2013, **4**, 1625–1628.

12 S. Ranjan, K. K. Zeming, R. Jureen, D. Fisher and Y. Zhang, *Lab Chip*, 2014, **14**, 4250–4262.

13 K. K. Zeming, T. Salafi, C. H. Chen and Y. Zhang, *Sci. Rep.*, 2016, **6**, 1–10.

14 M. Xavier, S. H. Holm, J. P. Beech, D. Spencer, J. O. Tegenfeldt, R. O. C. Oreffo and H. Morgan, *Lab Chip*, 2019, **19**, 513–523.

15 J. P. Beech and J. O. Tegenfeldt, *Lab Chip*, 2008, **8**, 657–659.

16 D. Di Carlo, D. Irimia, R. G. Tompkins and M. Toner, *Proc. Natl. Acad. Sci.*, 2007, **104**, 18892–18897.

17 M. Yamada, M. Nakashima and M. Seki, *Anal. Chem.*, 2004, **76**, 5465–5471.

18 T. Salafi, K. K. Zeming and Y. Zhang, *Lab Chip*, 2017, **17**, 11–33.

19 J. C. Contreras-Naranjo, H. J. Wu and V. M. Ugaz, *Lab Chip*, 2017, **17**, 3558–3577.

20 B. H. Wunsch, J. T. Smith, S. M. Gifford, C. Wang, M. Brink, R. L. Bruce, R. H. Austin, G. Stolovitzky and Y. Astier, *Nat. Nanotechnol.*, 2016, **11**, 936–940.

21 J. T. Smith, B. H. Wunsch, N. Dogra, M. E. Ahsen, K. Lee, K. K. Yadav, R. Weil, M. A. Pereira, J. V. Patel, E. A. Duch, J. M. Papalia, M. F. Lofaro, M. Gupta, A. K. Tewari, C. Cordon-Cardo, G. Stolovitzky and S. M. Gifford, *Lab Chip*, 2018, **18**, 3913–3925.

22 R. Devendra and G. Drazer, *Anal. Chem.*, 2012, **84**, 10621–10627.

23 J. P. Beech, P. Jönsson and J. O. Tegenfeldt, *Lab Chip*, 2009, **9**, 2698–2706.

24 J. P. Beech, K. Keim, B. D. Ho, C. Guiducci and J. O. Tegenfeldt, *Adv. Mater. Technol.*, 2019, **0**, 1900339.

25 V. Calero, P. Garcia-Sanchez, C. Honrado, A. Ramos and H. Morgan, *Lab Chip*, 2019, 1386–1396.

26 B. H. Lapizco-Encinas, *Electrophoresis*, 2018, 1–18.

27 L. Liang, Y. Ai, J. Zhu, S. Qian and X. Xuan, *J. Colloid Interface Sci.*, 2010, **347**, 142–146.

28 D. Hlushkou, R. K. Perdue, R. Dhopeshwarkar, R. M. Crooks and U. Tallarek, *Lab Chip*, 2009, **9**, 1903–1913.

29 B. Jung, R. Bharadwaj and J. G. Santiago, *Anal. Chem.*, 2006, **78**, 2319–2327.

30 S. S. Bahga and J. G. Santiago, *Analyst*, 2013, **138**, 735–754.

31 W. Y. Ng, A. Ramos, Y. C. Lam, I. P. Mahendra Wijaya and I. Rodriguez, *Lab Chip*, 2011, **11**, 4241–4247.

32 K. F. Warnick, S. J. Francom, P. H. Humble, R. T. Kelly, A. T. Woolley, M. L. Lee and H. D. Tolley, *Electrophoresis*, 2005, **26**, 405–414.